

Atomic controllable anchoring of uranium into zirconate pyrochlore with ultrahigh loading capacity†

Jian Sun,^{ab} Jing Zhou,^a Lili Li,^a Zhiwei Hu,^c Ting Shan Chan,^d Tonya Vitova,^e Sanzhao Song,^a Renduo Liu,^a Chao Jing,^a Haisheng Yu,^a Ming Zhang,^f Joerg Rothe,^{*e} Jian Qiang Wang ^{*ab} and Linjuan Zhang ^{*ab}

Efficient immobilization of actinide wastes is challenging in the nuclear energy industry. Here, we reported that 100% substitution of Zr^{4+} by U^{6+} in a $La_2Zr_2O_7$ matrix has been achieved for the first time by the molten salt (MS) method. Importantly, we observed that uranium can be precisely anchored into Zr or La sites of the $La_2Zr_2O_7$ matrix, as confirmed by X-ray diffraction, Raman, and X-ray absorption spectra. This work will guide the construction of site-controlled and high-capacity actinide-immobilized pyrochlore materials and could be extended to other perovskite materials.

Safe disposal of high-level nuclear wastes is a key issue for the development of nuclear power. Over the past three decades, significant efforts have been devoted to exploring the stable solid forms for the immobilization of high-level nuclear wastes in long-term geologic repositories. Zirconate pyrochlore (general formula $A_2B_2O_7$), which has good thermal stability, chemical durability and strong resistance to radiation damage, has been proposed as a superior host phase for nuclear wastes, especially for long-lived radioactive actinides.¹ Due to their ionic size, actinide ions could substitute on either the A site or B site in the $A_2B_2O_7$ host, which can directly alter the defect engineering and affect the stability of the immobilization host.² For instance, some A-site doped zirconate pyrochlore compounds such as $A_{2-x}An_xZr_2O_7$ ($A = La, Nd, Gd$; $An = Pu^{3+/4+}$,

$U^{4+/5+/6+}$) have been reported.^{2a-c,3} By contrast, Gregg and Zhang *et al.* reported that the uranium is mainly located on the pyrochlore B-site instead of the targeted A site.⁴ Some other B-site substituted $La_2Zr_{2-y}An_yO_7$ and $Gd_2Zr_{2-y}An_yO_7$ pyrochlores have also been reported.^{2d,5} In particular, the U oxidation state can be controlled under different sintering atmospheres.³ The incorporation of actinides into zirconate pyrochlore is generally achieved *via* several methods, such as the solid-state (SS) method,^{3,6} MS method,⁷ sol-gel method,⁸ co-precipitation method,^{1a} and gel-combustion method.⁹ Each method has its own advantages and shortcomings. For example, the conventional SS method normally requires sintering at temperatures above 1400 °C for more than 48 h to obtain pure pyrochlore phase,^{3,6,10} due to slow diffusion of the reacting constituents. Synthesis in the liquid phase or wet chemical conditions often requires environmentally unfriendly organic/inorganic precursors and solvents, such as chelating agents, and nitrates.^{1a,5a} Chemical synthesis methods of the materials play a vital role in adjusting the structure, size and phases and reducing the cost for industrial applications. Molten salts are promising synthesis media, because of their meritorious features, including environmental friendliness, low cost, being simple to operate, being easy to scale-up, *etc.*^{11,12} Previous works^{7,13} have reported the synthesis of pure $A_2B_2O_7$ phase by the MS method, suggesting that the MS method is feasible. Recently, we reported that uranium can precisely occupy the Nd or Zr sites to form $Nd_{2-x}U_xZr_2O_{7+\delta}$ ($0 \leq x \leq 0.2$) and $Nd_2Zr_{2-y}U_yO_{7+\delta}$ ($0 \leq y \leq 0.4$) nanoparticles.¹⁴ Here, we performed a systematic study of uranium accommodation in $La_2Zr_2O_7$ pyrochlore oxides *via* the MS method and achieved 100% substitution for the Zr site.

The synthesis of U-incorporated $La_2Zr_2O_7$ *via* the MS method is illustrated in Scheme S1 (ESI†). For comparison, we also synthesized the samples by the SS method with a calcination temperature of 1440 °C for 48 h. First, we compared the phase structure of undoped $La_2Zr_2O_7$ *via* the MS and SS method using conventional XRD (Fig. S1a, ESI†), synchrotron XRD (Fig. S2, ESI†)

^a Key Laboratory of Interfacial Physics and Technology, Shanghai Institute of Applied Physics, Chinese Academy of Sciences, Shanghai 201800, China.

E-mail: zhanglinjuan@sinap.ac.cn, wangjianqiang@sinap.ac.cn

^b University of Chinese Academy of Sciences, Beijing 100049, China

^c Max Planck Institute for Chemical Physics of Solids, Nothnitzer Strasse 40, Dresden 01187, Germany

^d National Synchrotron Radiation Research Center, 101 Hsin Ann Road, Hsinchu 30076, Taiwan, Republic of China

^e Karlsruhe Institute of Technology (KIT), Institute for Nuclear Waste Disposal (INE), Karlsruhe 76021, Germany. E-mail: rothe@kit.edu

^f Institute of Nuclear Science and Technology, Sichuan University, Chengdu 610064, China

† Electronic supplementary information (ESI) available. See DOI: 10.1039/d2cc00576j

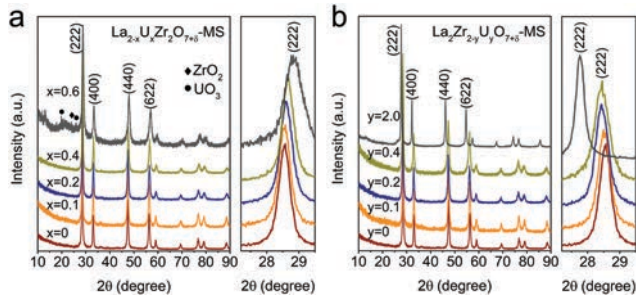


Fig. 1 XRD patterns for (a) $\text{La}_{2-x}\text{U}_x\text{Zr}_2\text{O}_{7+\delta}$ and (b) $\text{La}_2\text{Zr}_{2-y}\text{U}_y\text{O}_{7+\delta}$ samples synthesized by MS method. A magnified view of the diffraction peak corresponding to the (222) plane is also shown.

and Raman spectra (Fig. S1b, ESI[†]), supporting a typical pyrochlore structure (space group: $Fd\bar{3}m$) in $\text{La}_2\text{Zr}_2\text{O}_7$ host.

Next, we began to evaluate the solubility of uranium in $\text{La}_2\text{Zr}_2\text{O}_7$. Two series of U-doped $\text{La}_2\text{Zr}_2\text{O}_7$ oxides were prepared *via* the MS and SS method, targeting substitution on either the A-site forming $\text{La}_{2-x}\text{U}_x\text{Zr}_2\text{O}_{7+\delta}$ or B-site forming $\text{La}_2\text{Zr}_{2-y}\text{U}_y\text{O}_{7+\delta}$. As it is shown by XRD (Fig. S2c and S3, ESI[†]), for the series of U-doped $\text{La}_2\text{Zr}_2\text{O}_7$ -SS compounds, the pure pyrochlore phase persisted to $x \sim 0.1$, while $x \sim 0.2$ resulted in the formation of the second phase, such as ZrO_2 in the A-site-doped samples or $(\text{U}_{0.8}\text{La}_{0.2})\text{LaO}_4$ impurities in the B-site-doped samples. In contrast, in the $\text{La}_{2-x}\text{U}_x\text{Zr}_2\text{O}_{7+\delta}$ -MS samples, the second phases of ZrO_2 and UO_3 appear only when the U content rises to $x \sim 0.6$, while in the $\text{La}_2\text{Zr}_{2-y}\text{U}_y\text{O}_{7+\delta}$ -MS samples, no impurity peaks can be detected even when all B-site atoms are replaced by U atoms, reflecting that there is relatively higher U accommodation in the MS method. In addition, we clearly observed an opposite trend of the shift of diffraction lines shown in the right panel of Fig. 1a and b. In the $\text{La}_{2-x}\text{U}_x\text{Zr}_2\text{O}_{7+\delta}$ -MS samples, the diffraction peaks slightly shift towards higher 2θ angles, whereas they shift towards lower 2θ angles in the $\text{La}_2\text{Zr}_{2-y}\text{U}_y\text{O}_{7+\delta}$ -MS samples with increasing uranium content. A systematic shift in the peak position indicates a change in lattice parameters. Because the radius of the uranium ion is between those of La^{3+} (1.16 Å, 8-fold coordination) and Zr^{4+} (0.72 Å, 6-fold coordination) ions, the shrinkage or expansion of the lattice parameter is easy to understand when substituting La^{3+} or Zr^{4+} sites with uranium ions. In contrast, the shifts in the peak positions in the spectra of the U-doped $\text{La}_2\text{Zr}_2\text{O}_7$ -SS samples are random regardless of targeted substitution at the La^{3+} or Zr^{4+} sites, indicating that uranium ions cannot anchor in specific positions using the SS method. The lattice parameters are summarized in Table S1 (ESI[†]). Such structural evolution can also be confirmed by HR-TEM images (Fig. S4, ESI[†]). It is worth mentioning that the sample with full substitution of Zr with U was reported for the first time. To determine the precise cation ratio, ICP-MS analysis was carried out (Table S2, ESI[†]) and the element configuration was determined as $\text{La}_2\text{U}_{1.57}\text{O}_{7+\delta}$. XRD shows that the corresponding space group of the $\text{La}_2\text{U}_{1.57}\text{O}_{7+\delta}$ sample is $Fm\bar{3}m$, supporting the defective fluorite phase (Fig. 1b and Fig. S2b, ESI[†]). We also examined its atomic arrangement using a high-angle

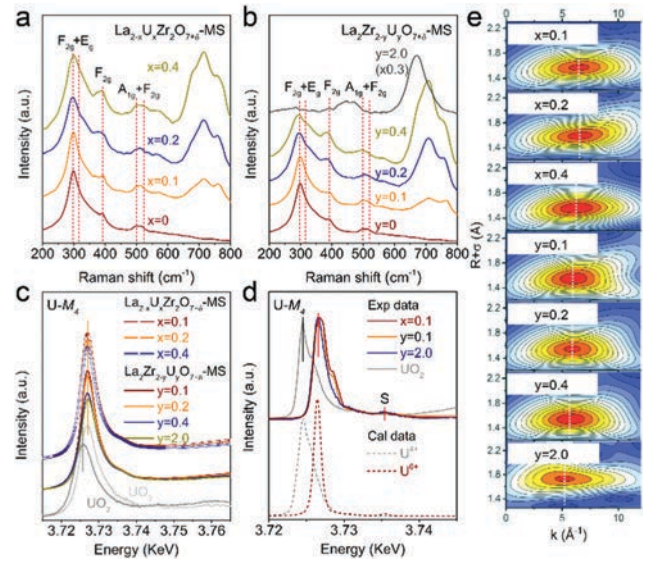


Fig. 2 Spectroscopic data of U doped $\text{La}_2\text{Zr}_2\text{O}_7$ samples for the MS method. Raman spectra of (a) $\text{La}_{2-x}\text{U}_x\text{Zr}_2\text{O}_{7+\delta}$ and (b) $\text{La}_2\text{Zr}_{2-y}\text{U}_y\text{O}_{7+\delta}$ samples. (c) U M_4 edge conventional XANES data, (d) U M_4 edge HERFD XANES data, and (e) the WT plot of the U L_3 edge for all samples.

annular-dark-field scanning transmission microscope (HAADF-STEM) in Fig. S5 (ESI[†]), which supports the pyrochlore phase of the $\text{La}_2\text{Zr}_2\text{O}_7$ sample and the fluorite phase of the $\text{La}_2\text{U}_{1.57}\text{O}_{7+\delta}$ sample. Raman spectroscopy was also used to observe the evolution of the crystal structure of the U-doped $\text{La}_2\text{Zr}_2\text{O}_7$ samples. Five Raman active vibrational features (Fig. 2a, b and Fig. S6, ESI[†]) can be observed in the U-doped $\text{La}_2\text{Zr}_2\text{O}_7$ samples, except $\text{La}_2\text{U}_{1.57}\text{O}_{7+\delta}$. In the $\text{La}_2\text{U}_{1.57}\text{O}_{7+\delta}$ sample, only a single broad Raman active mode in the range of $200\text{--}600\text{ cm}^{-1}$ can be observed (Fig. 2b), supporting the formation of the fluorite phase. The new broad peak in the region of $650\text{--}800\text{ cm}^{-1}$ in the U-doped $\text{La}_2\text{Zr}_2\text{O}_7$ samples is typical of highly disordered pyrochlore phases, and has been extensively reported in the literature¹⁵ on other pyrochlore materials disordered by high temperatures, pressures, and irradiation. In addition, the U^{6+} structure with UO_6 octahedral species may also contribute to this mode according to previous works.¹⁶ Combining XRD and Raman results, we can safely conclude that the MS method is firmly conducive to the higher accommodation of uranium in the $\text{La}_2\text{Zr}_2\text{O}_7$ pyrochlore phase, and most importantly, can accurately control the substitution position of the matrix.

X-Ray absorption spectra were used to investigate the local and electronic structure information around specific elements.¹⁷ First, the valence states of uranium ions in U-doped $\text{La}_2\text{Zr}_2\text{O}_7$ -MS samples are determined by the conventional U- M_4 edge X-ray absorption near-edge structure (XANES) spectra (Fig. 2c), in which the energy position of all U-doped samples is the same as that of UO_3 , indicating a U^{6+} oxidation state. In addition, uranium speciation can be evaluated through the comparisons of U- L_3 XANES spectra for the U-doped $\text{La}_2\text{Zr}_2\text{O}_7$ samples and other U-related references including UO_4^{2-} , UO_2^{2+} and UO_3 (Fig. S7b, ESI[†]). The U- L_3 white line

is very sensitive to the local coordination chemistry of the absorbing atom.¹⁸ The significant spectral differences between our samples and these references in Fig. S7b (ESI[†]) rules out the existence of uranium in the form of UO_4^{2-} , UO_2^{2+} and UO_3 , indicating that the possible species form is UO_6^{6-} in both A-site and B-site doped $\text{La}_2\text{Zr}_2\text{O}_7$ samples. Hexavalent uranium has an ionic radius of 0.73 Å and 0.86 Å in 6- and 8-fold coordination, respectively; these radii are comparable to that of Zr^{4+} (0.72 Å) but significantly smaller than that of La^{3+} (1.16 Å). Besides, due to the charge balance, U^{6+} doping at the La^{3+} sites is much more difficult. Thus, the A-site doped compound is prone to form the second phase at high U contents, which is consistent with the above XRD results. Due to the large lifetime broadening in conventional M_4 -edge XANES, no obvious pattern differences can be observed between $\text{La}_{2-x}\text{U}_x\text{Zr}_2\text{O}_{7+\delta}$ and $\text{La}_2\text{Zr}_{2-y}\text{U}_y\text{O}_{7+\delta}$ compounds.

Experimental resolution can be improved by high energy resolution fluorescence detection (HERFD) XANES.¹⁹ Fig. 2d shows the U- M_4 edge HERFD-XANES data of selected $\text{La}_{1.9}\text{U}_{0.1}\text{Zr}_2\text{O}_{7+\delta}$, $\text{La}_2\text{Zr}_{1.9}\text{U}_{0.1}\text{O}_{7+\delta}$ and $\text{La}_2\text{U}_{1.57}\text{O}_{7+\delta}$ samples synthesized by the MS method. The high-valent U^{6+} state mainly exists among all the synthesized samples, but significant differences were observed in A-site and B-site doped samples synthesized by the MS method for the first time using HERFD-XANES, whereas the spectral patterns are almost the same in corresponding samples synthesized by the SS method (Fig. S8, ESI[†]). It is worth noting that compared to the B-sites, which have octahedral UO_6 geometry, the ideal A site has a pentagonal bipyramidal UO_7 geometry; this discrepancy indicates a much higher local symmetry of U cations in the B-site doped samples. Fig. 2d shows that with increasing symmetry, the high-energy shoulder peak decreases until it disappears in $\text{La}_2\text{U}_{1.57}\text{O}_{7+\delta}$ -MS. In addition, a weak high-energy peak (marked by S) originating from the covalency between U^{6+} and O was observed among all U-doped samples, confirming the presence of a U^{6+} oxidation state. To probe the possible bonding between uranium and the oxygen ligand in the U-doped $\text{La}_2\text{Zr}_2\text{O}_7$, we performed extended X-ray absorption fine structure (EXAFS) analysis at the U L_3 -edge using both Fourier transform (FT) and wavelet transform (WT) analyses. The WT-EXAFS analysis²⁰ can provide the correlated structural information from both the R -space and k -space (Fig. 2e). The intensity maximum is well resolved for the $\text{La}_{2-x}\text{U}_x\text{Zr}_2\text{O}_{7+\delta}$ -MS ($\sim 6.5 \text{ \AA}^{-1}$) and $\text{La}_2\text{Zr}_{2-y}\text{U}_y\text{O}_{7+\delta}$ -MS ($\sim 5.8 \text{ \AA}^{-1}$) samples, arising from their differences in U-O bond lengths (Fig. S9b, ESI[†]). With increasing U doping, the structural disorder increases continuously. In particular, in extreme cases when all Zr atoms are replaced by uranium atoms, that is, $\text{La}_2\text{U}_{1.57}\text{O}_{7+\delta}$, the local structure displays significant changes both in the k^3 -weighted $\chi(k)$ and FT signals (Fig. S9, ESI[†]), as well as WT-contour plots (Fig. 2e), supporting the phase transformation in the $\text{La}_2\text{U}_{1.57}\text{O}_{7+\delta}$ compound, although no uranium- or lanthanum-derived oxides are evident from the XRD analysis. Zr-K XANES and EXAFS analysis (Fig. S10, ESI[†]) reveals that the local structure around the Zr atom remains unchanged with U doping.

To evaluate the relative stability of the possible U substitution in pristine $\text{La}_2\text{Zr}_2\text{O}_7$, we calculated the defect formation

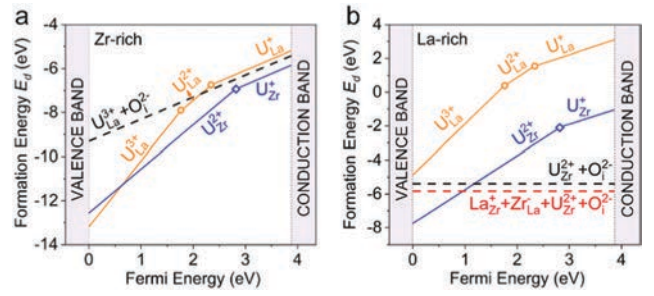


Fig. 3 The formation energies (E_d) of U point defects and possible U defect pairs as a function of the Fermi energy under (a) Zr rich and (b) La rich conditions. The Fermi energy (E_F) range corresponds to the calculated fundamental band gap of pristine $\text{La}_2\text{Zr}_2\text{O}_7$. The slope of the lines represents the charge state of the doping ions.

energies (E_d) for U substitutional La sites (U_{La}) and Zr sites (U_{Zr}), as shown in Fig. 3. According to the experiment, U-doped $\text{La}_2\text{Zr}_2\text{O}_7$ is prepared by replacing $\text{La}(\text{NO}_3)_3 \cdot 6\text{H}_2\text{O}$ and $\text{ZrO}(\text{NO}_3)_2 \cdot x\text{H}_2\text{O}$ with $\text{UO}_2(\text{NO}_3)_2 \cdot 6\text{H}_2\text{O}$, which suggests that $\text{La}_2\text{Zr}_2\text{O}_7$ bulk before doping is in the La vacancy and Zr vacancy states. The above two cases correspond to the Zr-rich and La-rich reference states. In Fig. 3a, when the E_F is near the VBM, the E_d of $\text{U}_{\text{La}}^{3+}$ is the lowest in all doping models, which indicates that high-valent U is most likely to exist in the form of $\text{U}_{\text{La}}^{3+}$ in $\text{La}_2\text{Zr}_2\text{O}_7$. Under La-rich conditions (Fig. 3b), $\text{U}_{\text{Zr}}^{2+}$, which has the lowest E_d , occurs at the E_F near the VBM, showing the stability of $\text{U}_{\text{Zr}}^{2+}$ defects. This conclusion implies that controlling the elemental component in the experiment is conducive to precisely controlling the U substitution position to form $\text{U}_{\text{La}}^{3+}$ or $\text{U}_{\text{Zr}}^{2+}$, which is consistent with the experimental conclusion mentioned above. It is believed that changing the E_F can simulate the effect of changes in dopant concentration.²¹ As reflected in Fig. 3a and b, the E_F increases and moves towards the CBM with increasing U doping concentration. Under Zr-rich conditions, with increasing E_F , the most stable $\text{U}_{\text{La}}^{3+}$ transfers to $\text{U}_{\text{Zr}}^{2+}$ defects at $E_F = 0.62 \text{ eV}$, indicating that with increasing U doping concentration, U could occupy the Zr site and that $\text{U}_{\text{Zr}}^{2+}$ becomes more energetically preferable. Thus, it is difficult to continue to form U_{La} defects with the high concentration of U doping; this conclusion is consistent with the experimental results shown in Fig. 1a; that is, it is difficult to achieve full occupation of U in the La sites to form $\text{U}_2\text{Zr}_2\text{O}_7$ material. Under La-rich conditions, the E_d of U_{Zr} is lower than that of all U_{La} defects, showing that U_{Zr} is more stable than U_{La} even at high U doping contents; this result is consistent with our XRD results.

In addition, the stable $\text{U}_{\text{La}}^{3+}$ and $\text{U}_{\text{Zr}}^{2+}$ inevitably have electrostatic interactions with other possible point defects with negative charges, such as La vacancies ($\text{V}_{\text{La}}^{3-}$), Zr vacancies ($\text{V}_{\text{Zr}}^{4-}$), and O interstices (O_i^{2-}), to maintain the charge balance of the whole system. Based on the total energy and E_d of $\text{U}_{\text{La}}^{3+} + \text{V}_{\text{La}}^{3-}$, $\text{U}_{\text{La}}^{3+} + \text{V}_{\text{Zr}}^{4-}$ and $\text{U}_{\text{La}}^{3+} + \text{O}_i^{2-}$ pairs and $\text{U}_{\text{Zr}}^{2+} + \text{V}_{\text{La}}^{3-}$, $\text{U}_{\text{Zr}}^{2+} + \text{V}_{\text{Zr}}^{4-}$ and $\text{U}_{\text{Zr}}^{2+} + \text{O}_i^{2-}$ pairs (Table S3 and Fig. S11, ESI[†]), we compared the E_d between U point defects and possible U defect pairs in Fig. 3. As shown in Fig. 3a, $\text{U}_{\text{La}}^{3+} + \text{O}_i^{2-}$ is the

most stable and has the lowest E_d when the E_F is above 2.28 eV, suggesting that U_{La}^{3+} tends to combine with O_i^{2-} to form defective pairs with increasing U doping concentration. In Fig. 3b, $U_{Zr}^{2+} + O_i^{2-}$ is most stable at E_F above 1.38 eV, implying that the introduction of O_i can significantly reduce the formation energy of the whole system when doping with high U contents. Considering that the MS method is conducive to supplying oxygen due to its faster mass transport ability, it is easier to synthesize pure pyrochlore samples with high U content using the MS method, as theoretically predicted. Moreover, to investigate the possibility of fluorite phase formation, we also calculated the E_d of anti-site defects ($La_{Zr}^- + Zr_{La}^+$) and constructed a $La_{Zr}^- + Zr_{La}^+ + U_{Zr}^{2+} + O_i^{2-}$ defect cluster. As shown in Fig. 3b, the E_d of $La_{Zr}^- + Zr_{La}^+ + U_{Zr}^{2+} + O_i^{2-}$ was 0.35 eV lower than that of $U_{Zr}^{2+} + O_i^{2-}$, indicating that the fluorite phase is more likely to exist when high concentration U is doped. This conclusion is consistent with the experimental result that fluorite $La_2U_2O_{7+\delta}$ is finally formed.

In summary, we systematically studied the uranium solubility, species, valence state and defects in $La_2Zr_2O_7$ pyrochlore synthesized by the MS method. Compared to the SS method, the MS method is of prime significance for the ultrahigh loading capacity of uranium ions and of precisely controlling the U substitution into La or Zr sites in $La_2Zr_2O_7$. This work will guide the construction of site-controlled and high-capacity actinide-immobilized pyrochlore materials and could be extended to other materials (Fig. S12, ESI[†]).

This work is in celebration of the 10th Anniversary of the Founding of the Youth Innovation Promotion Association of the Chinese Academy of Sciences. The authors are grateful for the financial support from the “Transformational Technologies for Clean Energy and Demonstration,” Strategic Priority Research Program of the Chinese Academy of Sciences (Grant No. XDA2100000), the K. C. Wong Education Foundation (GJTD-2018-10), Youth Innovation Promotion Association, Chinese Academy of Science (No. Y201842), the National Science Foundation of China (No. 21876183, 21771133) and Instrument and Equipment Development Program Chinese Academy of Science (No. YJKYYQ20180066). We acknowledge the support from the beamlines 14W1 of the Shanghai Synchrotron Radiation Facility (SSRF), the Max Planck-POSTECH-Hsinchu Center for Complex Phase Materials, the KIT light source for the provision of instruments at the CAT-ACT beamline and KIT-IBPT for the operation of the KARA storage ring.

Conflicts of interest

There are no conflicts to declare.

Notes and references

- (a) S. Finkeldei, M. C. Stennett, P. M. Kowalski, Y. Ji, E. de Visser Týnová, N. C. Hyatt, D. Bosbach and F. Brandt, *J. Mater. Chem. A*, 2020, **8**, 2387–2403; (b) R. Perriot, P. P. Dholabhai and B. P. Uberuaga, *Phys. Chem. Chem. Phys.*, 2016, **18**, 22852–22863; (c) R. Perriot and B. P. Uberuaga, *J. Mater. Chem. A*, 2015, **3**, 11554–11565; (d) K. E. Sickafus, R. W. Grimes, J. A. Valdez, A. Cleave, M. Tang, M. Ishimaru, S. M. Corish, C. R. Stanek and B. P. Uberuaga, *Nat. Mater.*, 2007, **6**, 217–223.
- (a) C. Naestren, R. Jardin, J. Somers, M. Walter and B. Brendebach, *J. Solid State Chem.*, 2009, **182**, 1–7; (b) D. J. Gregg, Y. Zhang, S. C. Middleburgh, S. D. Conradson, G. Triani, G. R. Lumpkin and E. R. Vance, *J. Nucl. Mater.*, 2013, **443**, 444–451; (c) S. K. Gupta, C. Reghukumar, N. Pathak, K. Sudarshan, D. Tyagi, M. Mohapatra, P. K. Pujari and R. M. Kadam, *Chem. Phys. Lett.*, 2017, **669**, 245–250; (d) H. Y. Xiao, M. Jiang, F. A. Zhao, Z. J. Liu and X. T. Zu, *J. Nucl. Mater.*, 2015, **466**, 162–171.
- D. J. Gregg, Y. Zhang, Z. Zhang, I. Karatchevtseva, M. G. Blackford, G. Triani, G. R. Lumpkin and E. R. Vance, *J. Nucl. Mater.*, 2013, **438**, 144–153.
- (a) D. J. Gregg, Z. Zhang, G. J. Thorogood, B. J. Kennedy, J. A. Kimpton, G. J. Griffiths, P. R. Guagliardo, G. R. Lumpkin and E. R. Vance, *J. Nucl. Mater.*, 2014, **452**, 474–478; (b) F. X. Zhang, M. Lang, C. Tracy, R. C. Ewing, D. J. Gregg and G. R. Lumpkin, *J. Solid State Chem.*, 2014, **219**, 49–54.
- (a) K. V. G. Kutty, R. Asuvathraman, R. R. Madhavan and H. Jena, *J. Phys. Chem. Solids*, 2005, **66**, 596–601; (b) R. E. Williford and W. J. Weber, *J. Nucl. Mater.*, 2001, **299**, 140–147.
- (a) X. Shu, L. Fan, X. Lu, Y. Xie and Y. Ding, *J. Eur. Ceram. Soc.*, 2015, **35**, 3095–3102; (b) X. Shu, X. Lu, L. Fan, R. Yang, Y. Ding, S. Pan, P. Zhou and Y. Wu, *J. Mater. Sci.*, 2016, **51**, 5281–5289.
- Y. Mao, X. Guo, J. Y. Huang, K. L. Wang and J. P. Chang, *J. Phys. Chem. C*, 2009, **113**, 1204–1208.
- Z. Tang, Z. Huang, W. Han, J. Qi, Y. Shi, N. Ma, Y. Zhang, X. Guo and T. Lu, *Inorg. Chem.*, 2020, **59**, 9919–9926.
- (a) M. Mohapatra, B. Rajeswari, N. S. Hon and R. M. Kadam, *Luminescence*, 2016, **31**, 1519–1523; (b) S. K. Gupta, C. Reghukumar, M. Keskar and R. M. Kadam, *J. Lumin.*, 2016, **177**, 166–171.
- X. Lu, C. Hou, Y. Xie, X. Shu, Y. Ding, D. Ma, W. Ren and L. Bian, *Ceram. Int.*, 2017, **43**, 3015–3024.
- S. K. Gupta and Y. Mao, *Prog. Mater. Sci.*, 2021, **117**, 100734.
- X. Liu, N. Fechner and M. Antonietti, *Chem. Soc. Rev.*, 2013, **42**, 8237–8265.
- (a) Z. Huang, F. Li, C. Jiao, J. Liu, J. Huang, L. Lu, H. Zhang and S. Zhang, *Ceram. Int.*, 2016, **42**, 6221–6227; (b) X. Wang, Y. Zhu and W. Zhang, *J. Non Cryst. Solids*, 2010, **356**, 1049–1051.
- J. Sun, J. Zhou, Z. Hu, T. S. Chan, R. Liu, H. Yu, L. Zhang and J. Q. Wang, *J. Synchrotron Radiat.*, 2022, **29**, 37–44.
- (a) M. Lang, F. Zhang, J. Zhang, J. Wang, J. Lian, W. J. Weber, B. Schuster, C. Trautmann, R. Neumann and R. C. Ewing, *Nucl. Instrum. Methods Phys. Res., Sect. B*, 2010, **268**, 2951–2959; (b) K. M. Turner, D. R. Rittman, R. A. Heymach, C. L. Tracy, M. L. Turner, A. F. Fuentes, W. L. Mao and R. C. Ewing, *J. Phys.: Condens. Matter*, 2017, **29**, 255401; (c) C. L. Tracy, J. Shamblin, S. Park, F. Zhang, C. Trautmann, M. Lang and R. C. Ewing, *Phys. Rev. B*, 2016, **94**, 064102.
- (a) M. L. Palacios and S. H. Taylor, *Appl. Spectrosc.*, 2000, **54**, 1372–1378; (b) K. Popa, D. Prieur, D. Manara, M. Naji, J. F. Vigier, P. M. Martin, O. D. Blanco, A. C. Scheinost, T. Pruessmann, T. Vitova, P. E. Raison, J. Somers and R. J. M. Konings, *Dalton Trans.*, 2016, **45**, 7847–7855.
- Q. Gu and H. H. Wen, *Innovation*, 2022, **3**, 100202.
- E. A. Hudson, J. J. Rehr and J. J. Bucher, *Phys. Rev. B: Condens. Matter Mater. Phys.*, 1995, **52**, 13815–13826.
- (a) K. O. Kvashnina, S. M. Butorin, P. Martin and P. Glatzel, *Phys. Rev. Lett.*, 2013, **111**, 253002; (b) T. Vitova, I. Pidchenko, S. Biswas, G. Beridze, P. W. Dunne, D. Schild, Z. Wang, P. M. Kowalski and R. J. Baker, *Inorg. Chem.*, 2018, **57**, 1735–1743; (c) J. Rothe, S. Butorin, K. Dardenne, M. A. Denecke, B. Kienzler, M. Loeble, V. Metz, A. Seibert, M. Steppert, T. Vitova, C. Walther and H. Geckeis, *Rev. Sci. Instrum.*, 2012, **83**, 043105; (d) Y. Podkovyryna, I. Pidchenko, T. Pruessmann, S. Bahl, J. Goettlicher, A. Soldatov and T. Vitova, *J. Phys.: Conf. Ser.*, 2015, **712**, 012092.
- H. Funke, M. Chukalina and A. C. Scheinost, *J. Synchrotron Radiat.*, 2007, **14**, 426–432.
- H. X. Xu, D. Lee, J. He, S. B. Sinnott, V. Gopalan, V. Dierolf and S. R. Phillpot, *Phys. Rev. B: Condens. Matter Mater. Phys.*, 2008, **78**, 174103.

Repository KITopen

Dies ist ein Postprint/begutachtetes Manuskript.

Empfohlene Zitierung:

Sun, J.; Zhou, J.; Li, L.; Hu, Z.; Chan, T.-S.; Vitova, T.; Song, S.; Liu, R.; Jing, C.; Yu, H.; Zhang, M.; Rothe, J.; Wang, J.-Q.; Zhang, L.

[Atomic controllable anchoring of uranium into zirconate pyrochlore with ultrahigh loading capacity](#)

2022. Chemical Communications, 58.

doi: [10.5445/IR/1000143446](https://doi.org/10.5445/IR/1000143446)

Zitierung der Originalveröffentlichung:

Sun, J.; Zhou, J.; Li, L.; Hu, Z.; Chan, T.-S.; Vitova, T.; Song, S.; Liu, R.; Jing, C.; Yu, H.; Zhang, M.; Rothe, J.; Wang, J.-Q.; Zhang, L.

[Atomic controllable anchoring of uranium into zirconate pyrochlore with ultrahigh loading capacity](#)

2022. Chemical Communications, 58 (21), 3469–3472.

doi:[10.1039/d2cc00576j](https://doi.org/10.1039/d2cc00576j)

Lizenzinformationen: [KITopen-Lizenz](#)